electronics

MDPI

Article

A Low-Profile Beam-Scanning Antenna Array for 5G Low-Cost Millimeter-Wave Applications

Guan-Long Huang [1], Ming-Feng Xu [1], Jing Wu [1], Zi-Yu Pang [2], Yan-Ji Chen [3], Chow-Yen-Desmond Sim [4,*], Wei Lin [5], Su-Wei Chang [6] and Yiannis Vardaxoglou [7]

[1] School of Electronic and Information Engineering, Foshan University, Foshan 528225, China; hgl@fosu.edu.cn (G.-L.H.); 2112353014@stu.fosu.edu.cn (M.-F.X.); 2112353012@stu.fosu.edu.cn (J.W.)
[2] Department of Electrical and Computer Engineering, University of Macau, Macau SAR 999078, China; yc27461@um.edu.mo
[3] Department of Electrical Engineering, Feng Chia University, Taichung 40724, Taiwan; m0705982@fcu.edu.tw
[4] Department of Electrical Engineering, National Sun Yat-Sen University, Kaohsiung 804201, Taiwan
[5] Department of Electrical and Electronic Engineering, The Hong Kong Polytechnic University, Hong Kong SAR 999077, China; w.lin@polyu.edu.hk
[6] TMY Technology Inc., New Taipei City 220056, Taiwan; swchang@tmytek.com
[7] School of Microelectronics, South China University of Technology, Guangzhou 510641, China; yiannisvardax@ieee.org
* Correspondence: cysim@ieee.org

Abstract

A low-profile beam-scanning antenna array for cost-effective 5G millimeter-wave (mmWave) applications is proposed in this work. The array features a compact single-layer substrate structure while achieving a wide operating bandwidth covering the 5G n257 band (26.5–29.5 GHz). A novel antenna element is first designed and analyzed, employing a metallic rectangular patch with shorting pins as the radiator, excited through a modified coplanar waveguide (CPW) feeding structure. Based on this element, four-element and eight-element linear arrays are developed with an overall profile of only 0.07 λ at 28 GHz and fabricated to experimentally assess beam-scanning performance. To accurately characterize and validate the radiation behavior, an mmWave beam box system is utilized for pattern measurements. The results demonstrate that the fabricated arrays achieve an impedance bandwidth fully covering the 5G n257 band with VSWR < 2, while the measured beam-scanning performance closely agrees with simulations. These findings confirm that the proposed design and its extensions offer strong potential for practical integration into future 5G mmWave communication devices.

Keywords: 5G antenna; beam-scanning; low-cost; low-profile; millimeter-wave antenna

Academic Editors: Yuanxi Cao and Hailiang Zhu

Received: 19 July 2025
Revised: 24 August 2025
Accepted: 25 August 2025
Published: 29 August 2025

Citation: Huang, G.-L.; Xu, M.-F.; Wu, J.; Pang, Z.-Y.; Chen, Y.-J.; Sim, C.-Y.-D.; Lin, W.; Chang, S.-W.; Vardaxoglou, Y. A Low-Profile Beam-Scanning Antenna Array for 5G Low-Cost Millimeter-Wave Applications. *Electronics* **2025**, *14*, 3453. https://doi.org/10.3390/electronics14173453

1. Introduction

Fifth-generation (5G) communication systems are currently undergoing intensive research and development in both academia and industry. Compared with existing systems, 5G is envisioned to deliver superior performance, including higher data rates, improved spectral efficiency, and enhanced reliability. Two primary frequency ranges have been defined for 5G: the sub-6 GHz band (FR1) and the millimeter-wave (mmWave) band (FR2). While the sub-6 GHz band primarily supports wide-area coverage, the mmWave band is intended to enable ultra-high-speed data transmission for future industrial applications. Antennas are recognized as critical components in the realization of 5G technology, leading to extensive research efforts in areas such as massive multiple-input multiple-output (MIMO) antenna arrays in both FR1

and FR2 bands [1–4], antenna decoupling methods for mobile communications [5–7], mmWave antenna/array designs for mobile terminals [8–10], and antenna-in-package (AiP) solutions with integrated front-end modules [11,12]. In particular, multilayer antenna structures are often adopted to achieve wide operating bandwidths at mmWave frequencies. However, such configurations inevitably increase the overall profile, fabrication complexity, and cost.

In addition to antenna design strategies, most emerging 5G antenna technologies face limitations in measurement and characterization. Real-time evaluation of mmWave beam-scanning performance remains challenging, as conventional testing methods are inadequate. Figure 1 illustrates a representative 5G mmWave transceiver architecture for dynamic beamforming, which typically consists of a baseband module, up/down (U/D) converter, beamformer, and antenna. Among these components, the beamformer plays a central role in beam-scanning evaluation. Yet, in the absence of costly in-house RF front-end testing systems, many reported works assess the beamforming capability of customized mmWave arrays solely through simulations or post-processed measurements of individual antenna elements [9]. Furthermore, integrating beamformers or RFICs in mmWave and massive MIMO systems poses significant challenges, as high-density packaging and antenna integration must balance performance enhancement with device miniaturization. Insufficient isolation and excessive mutual coupling can introduce signal distortion and beam-steering errors, while packaging and interconnect techniques must maintain low insertion loss and good impedance matching to preserve system integrity. Consequently, the development of cost-effective, reliable, and repeatable 5G mmWave antenna testing platforms remains an open problem that requires further research attention.

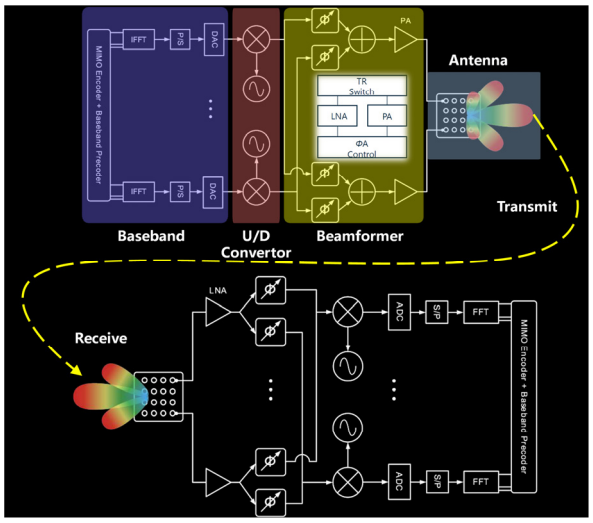

Figure 1. Fifth-generation mmWave transceiver circuit architecture for beamforming.

To address these challenges, this paper proposes a low-profile, beam-scanning antenna array with a simple structure for cost-efficient 5G mmWave applications. The array is realized on a single-layer printed circuit board (PCB) and operates across the 5G n257 band (26.5–29.5 GHz). Moreover, to overcome the difficulties in experimentally characterizing real-time beam-scanning performance, a recently developed measurement instrument, the beam box, is employed to evaluate the radiation patterns of the proposed array.

2. Antenna Array Design and Analysis

2.1. Antenna Element Configuration

The configuration of the proposed mmWave antenna element is illustrated in Figure 2. The element is implemented on a single-layer Rogers RO4350 (Chandler, AZ, USA) substrate with a thickness of 0.762 mm, a dielectric constant of 3.66, and a loss tangent of 0.004. The

primary radiator is a rectangular patch with dimensions of 5.18 mm (W_p) × 2.9 mm (L_p), printed on the top surface of the substrate. The patch is excited through a metallic via (Φ_1 = 0.6 mm, referred to as the central pin) that connects to a modified coplanar waveguide (CPW) feedline printed on the bottom surface. This modified CPW, incorporating a Π-shaped slot, functions analogously to a CPW capacitive feed, effectively reducing the antenna's profile along the *y*-axis. In addition, two auxiliary shorting pins (Φ_2 = 0.3 mm, termed side pins) are inserted symmetrically along the patch edges, enabling the excitation of two adjacent resonant modes at approximately 26.9 GHz and 29.8 GHz. The combination of these modes produces a continuous impedance bandwidth covering the 5G n257 band.

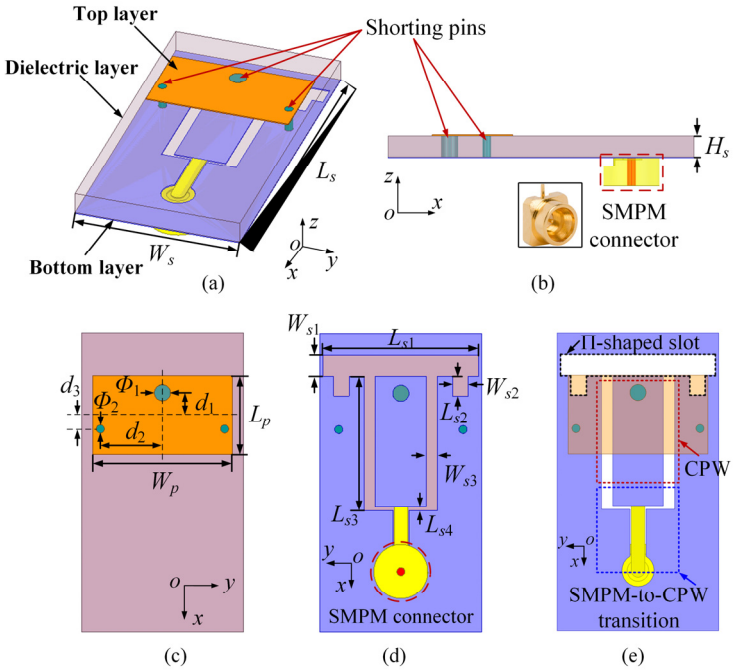

Figure 2. Fifth-generation mmWave transceiver circuit architecture for beamforming. Detailed configuration of the antenna unit. (**a**) Three-dimensional view. (**b**) Side view. (**c**) Top view (ground plane hidden). (**d**) Bottom view (top layer hidden). (**e**) Top view marked with detailed structures.

To accommodate high-frequency measurements, an SMPM surface-mount connector is employed instead of the conventional SMA connector, which suffers from excessive loss at mmWave frequencies, as shown in Figure 2b. Accordingly, an SMPM-to-CPW transition is designed on the bottom layer of the substrate to ensure proper integration, as depicted in Figure 2e. Electromagnetic simulations of the antenna unit are performed using HFSS® 2021. The simulated reflection coefficient and radiation patterns at 28 GHz are presented in Figure 3a–c. The results confirm that the antenna achieves wideband operation across 26.5–29.5 GHz with a reflection coefficient below −10 dB and exhibits a peak gain of approximately 5.5 dBi. The overall physical size of the antenna element is 11 mm (*Ls*) × 6 mm (*Ws*). A summary of the geometrical parameters is provided in Table 1.

Table 1. Parameter dimensions of the antenna unit (Unit: mm).

Parameter	Value	Parameter	Value	Parameter	Value
L_S	11.0	d_1	25	L_{S3}	4.92
H_S	0.762	d_3	25	W_{S1}	0.77
W_P	5.18	Φ_2	38	W_{S3}	0.42
L_{S2}	0.73	W_S	38	d_2	2.3
L_{S4}	0.14	L_P	9	Φ_1	0.6
W_{S2}	0.58	L_{S1}	2	s	6.0

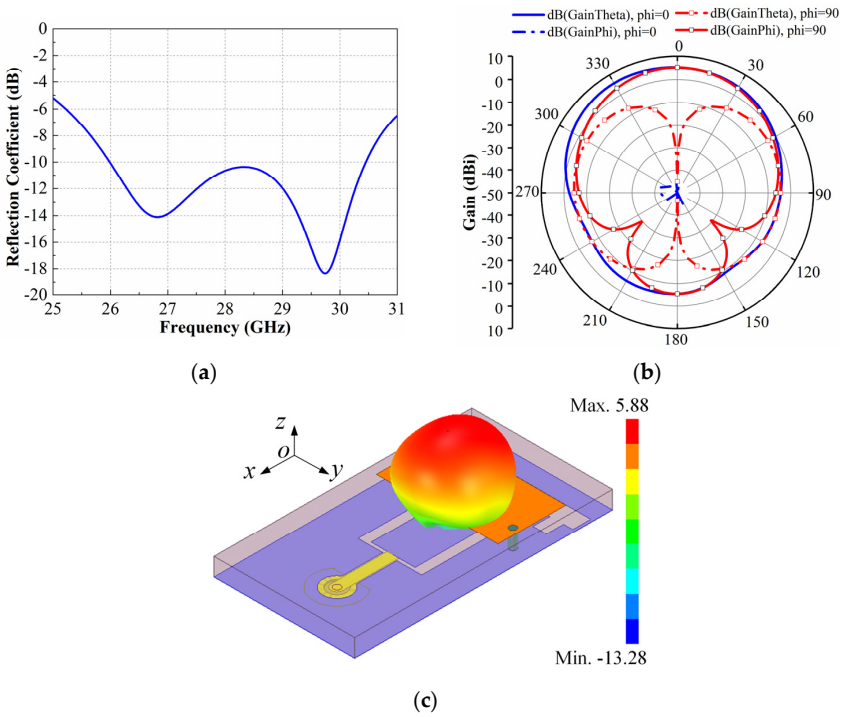

Figure 3. Simulated results of the antenna unit. (**a**) Reflection coefficient. (**b**) Two-dimensional radiation pattern at 28 GHz. (**c**) Three-dimensional radiation pattern at 28 GHz.

2.2. Antenna Working Mechanism

To further elucidate the operating principle of the proposed antenna element, the surface current distributions at the two resonant frequencies, 26.9 GHz and 29.8 GHz, are illustrated in Figure 4a,b, respectively. It can be observed that the dominant current flow at both resonances, after vector superposition, is primarily aligned along the *x*-axis, confirming that the antenna achieves stable linear polarization. The design evolution and the underlying mechanism for bandwidth enhancement are summarized in Figure 5. For a conventional probe-fed patch antenna without shorting vias, only a narrow resonance at a higher frequency (30.5 GHz) is obtained [Figure 5a]. By introducing the CPW feed structure with embedded slots on the ground plane, an additional resonance is coupled to the patch at a lower frequency (26.9 GHz), as shown in Figure 5b.

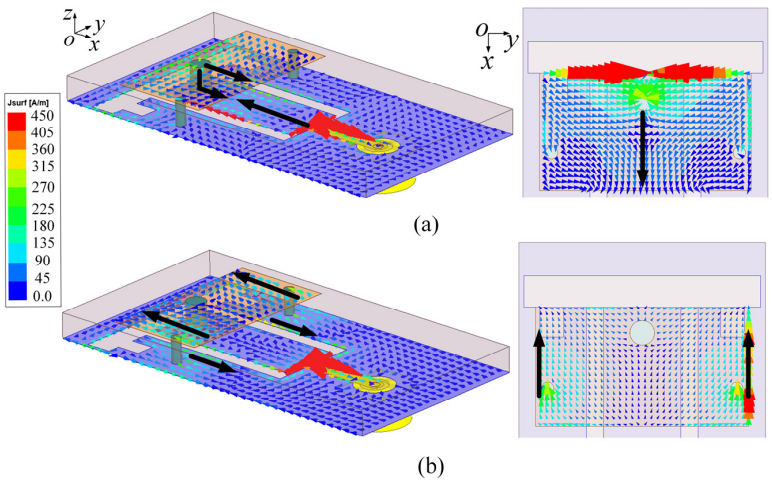

Figure 4. Simulated current distribution of the antenna unit. (**a**) Current distribution at 26.9 GHz. (**b**) Current distribution at 29.8 GHz.

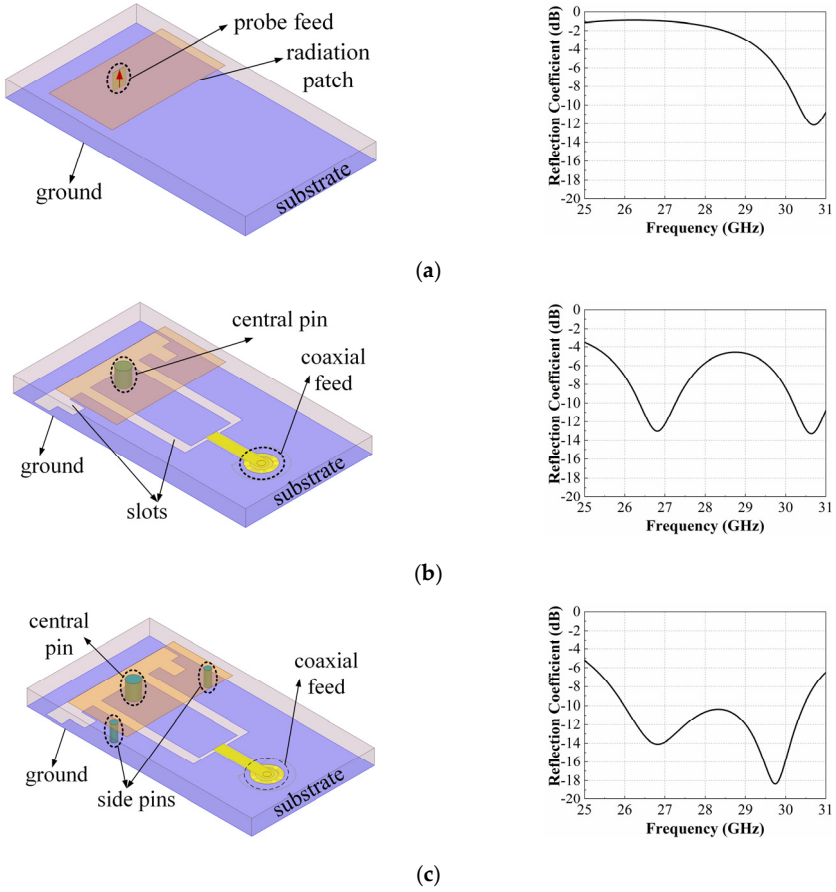

Figure 5. Design evolution of the antenna unit. (**a**) Antenna unit configuration without any via. (**b**) Antenna unit configuration with a central-fed via. (**c**) A central-fed antenna unit configuration with two side vias.

To merge the two initially separated resonances and realize wideband impedance matching across the n257 band, two shorting pins are symmetrically placed on both sides of the radiating patch [Figure 5c]. These pins not only improve impedance matching but also extend the effective current path of the higher-order resonance, thereby lowering its frequency from 30.5 GHz to 29.8 GHz in the optimized design, while the lower resonance induced by the CPW slots remains nearly unaffected.

Considering the compactness of the CPW feed structure, sensitivity to fabrication tolerances is also investigated. Figure 6 shows the impact of varying the microstrip feed-line width (*fw*) on the reflection coefficient. The results indicate that increasing *fw* shifts the resonant frequencies toward lower values, while the overall impedance response remains consistent.

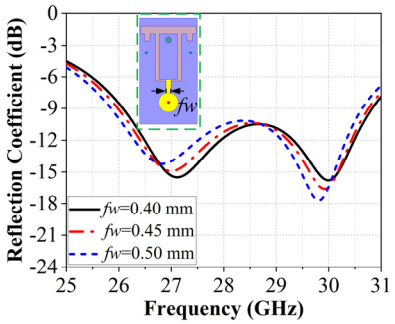

Figure 6. Simulated reflection coefficients with different *fw*.

2.3. Antenna Array Beam-Scanning Performance

To evaluate the array performance, a four-element linear mmWave antenna array, derived from the proposed antenna element, is designed with an inter-element spacing of s = 6 mm ($0.56\lambda_{28GHz}$), as illustrated in Figure 7. The simulated scattering parameters (S-parameters) of this array are presented in Figure 8a. To avoid ambiguity among the coupling curves corresponding to different ports, only representative cases are shown, including the worst-case mutual coupling between adjacent elements. The results indicate that the array operates effectively across the n257 band, with mutual coupling levels below −12 dB. This relatively low coupling, mainly attributed to the half-wavelength inter-element spacing, preserves spatial independence among the antenna units, thereby improving spatial multiplexing gain and overall system capacity. Furthermore, reduced mutual coupling minimizes distortion of the array factor, ensuring stable main-lobe steering, effective sidelobe suppression, uniform transmit power distribution, and reliable link quality in massive MIMO deployments.

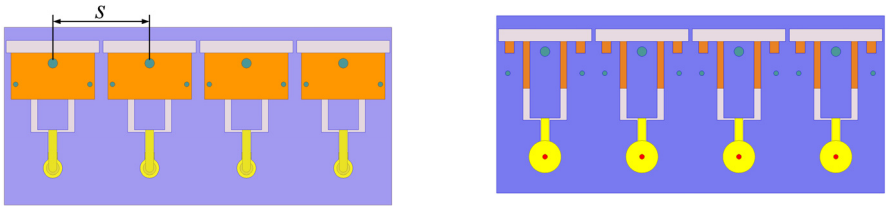

(**a**) (**b**)

Figure 7. Configuration of the four-element antenna array in element spacing of S = 6 mm. (**a**) Top view. (**b**) Bottom view.

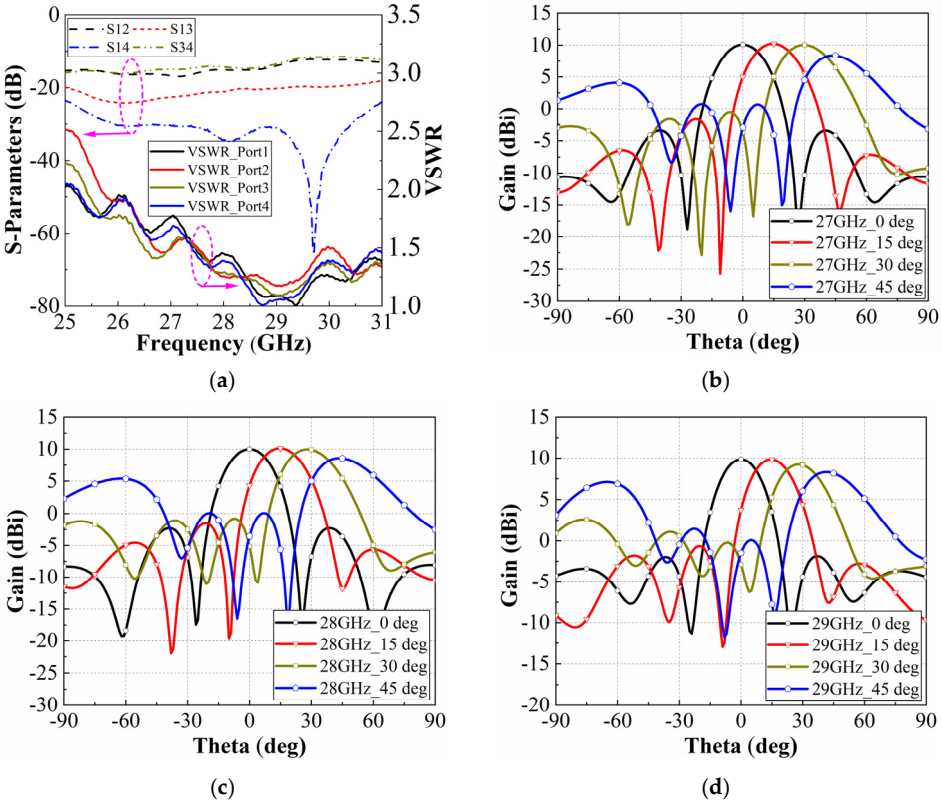

(**a**) (**b**) (**c**) (**d**)

Figure 8. Simulated results of the four-element antenna array. (**a**) S-parameters. Beam-steering at (**b**) 27 GHz, (**c**) 28 GHz, and (**d**) 29 GHz.

The beam-scanning performance of the four-element array is further investigated by exciting the elements with different phase progressions. The simulated radiation patterns

at 27 GHz, 28 GHz, and 29 GHz for scanning angles of 0°, 15°, 30°, and 45° in the *y*-direction are shown in Figure 8b–d. The results demonstrate stable beam-steering with a maximum gain of approximately 10 dBi at boresight, which is slightly lower than the expected 11 dBi due to dielectric losses and potential measurement uncertainties. The gain performance remains nearly constant for scanning angles up to 30°, while a noticeable drop is observed beyond 45°, suggesting that tapering or other sidelobe reduction techniques may be beneficial for further optimization.

To provide a more intuitive representation, Figure 9 illustrates the three-dimensional (3D) beam tilting characteristics at the aforementioned scanning angles. In addition, as eight-element phased arrays are highly desirable for future 5G mm Wave systems, the proposed design is further extended to an eight-element configuration. The corresponding numerical results confirm similar radiation characteristics to those of the four-element array, thereby validating the scalability and robustness of the proposed design.

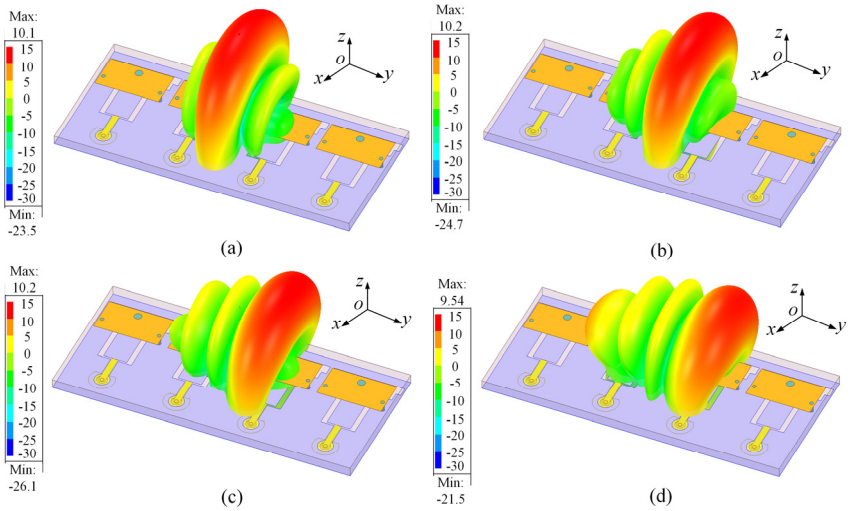

Figure 9. Three-dimensional beam tilting performance of the four-element antenna array at 28 GHz. Beam tilting at (**a**) 0°, (**b**) 15°, (**c**) 30°, and (**d**) 45°.

3. Fabrication and Measurement

The proposed antenna array is fabricated on a single-layer Rogers RO4350 substrate with a thickness of 0.762 mm, a dielectric constant of 3.66, and a loss tangent of 0.004. Conventional multilayer PCB fabrication not only requires additional dielectric substrates but also adhesive layers between them. Such a process involves multiple fabrication steps, which significantly increase production cost. Similarly, antenna-in-package (AiP) technology relies on expensive packaging materials and complex procedures, while testing often requires specialized probe stations or over-the-air (OTA) anechoic chambers, further elevating the cost. In contrast, the antenna array presented in this work is directly implemented on a single-layer PCB, thereby eliminating complicated processing steps and achieving a compact structure with reduced cost.

Photographs of the fabricated four-element and eight-element prototypes are shown in Figure 10. During S-parameter measurements, surface-mounted SMPM connectors were soldered to the pads on the bottom PCB layer, and the prototypes were tested using a Keysight N5225a PNA (Santa Rosa, CA, USA) (10 MHz–50 GHz) via SMPM-to-K cables. Matching loads were applied to the inactive ports during measurement. Evaluation of beam-scanning performance requires radiation pattern measurements in an anechoic chamber, where all array elements must be excited with appropriate phase progressions corresponding to specific scanning angles. However, traditional chambers typically support only a single feed cable for the antenna under test (AUT). Although customized

feed networks with phase-shifting circuits can be used, such an approach is cumbersome, time-consuming, and unable to provide real-time dynamic beam-steering.

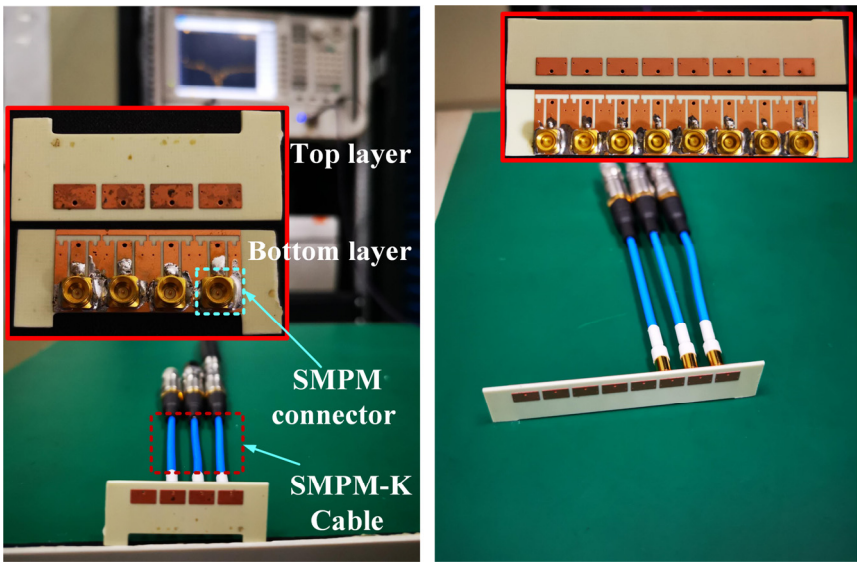

Figure 10. Prototypes of the proposed four- and eight-antenna arrays.

In particular, it is challenging to realize a practical phase-shifting test kit at the mmWave band. To address this, a multiport phase generator, namely the beam box (BBox) [13], was employed in this work, as illustrated in Figure 11a. The selected BBox provides 16 SMPM ports/channels operating within 24–31 GHz, with a 6-bit phase resolution offering full 360° coverage and a 5-bit attenuation range up to 35 dB. SMPM-to-SMPM coaxial cables were used to connect the arrays to the BBox. Both four- and eight-element arrays were tested in a mmWave anechoic chamber, as shown in Figure 11b,c.

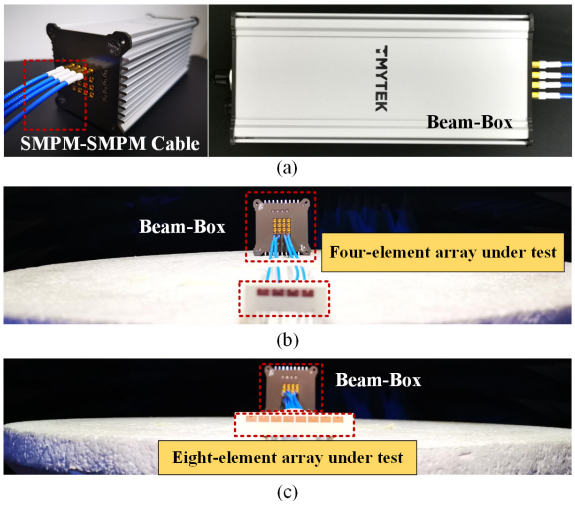

Figure 11. Measurement setup of the proposed antenna arrays. (**a**) Beam box with SMPM-to-SMPM cable connection. (**b**) Four-element array under test in chamber. (**c**) Eight-element array under test in chamber.

The measured S-parameters and beam-steering patterns of the arrays are presented in Figures 12 and 13, respectively, showing good agreement with simulation. Both arrays achieve stable operation across the 5G mmWave n257 band (26.5–29.5 GHz) with VSWR < 2.0 and port isolation better than 12 dB. Furthermore, satisfactory beam-steering characteristics were observed, with consistent radiation patterns across the band of interest. As expected, higher sidelobe levels appear at large scanning angles, which could

be mitigated in future implementations by employing amplitude tapering techniques. Figure 13e further depicts the simulated and measured radiation efficiencies, demonstrating values above 80% within the operating band. The slightly lower measured efficiency is mainly attributed to practical factors such as dielectric and conductor losses. The proposed antenna array has the advantages of wider bandwidth and lower profile compared with the published work, as shown in Table 2. These results confirm that the proposed array provides excellent performance and is a strong candidate for 5G mmWave applications.

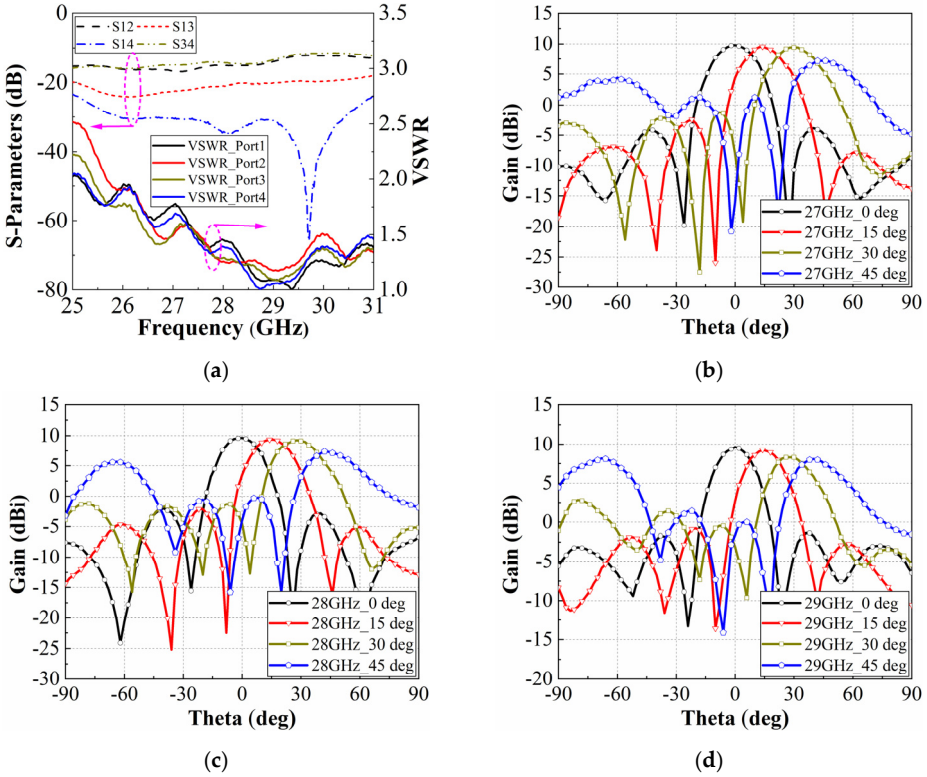

Figure 12. Measured results of the four-element antenna array. (**a**) S-parameters. Beam-steering at (**b**) 27 GHz, (**c**) 28 GHz, and (**d**) 29 GHz.

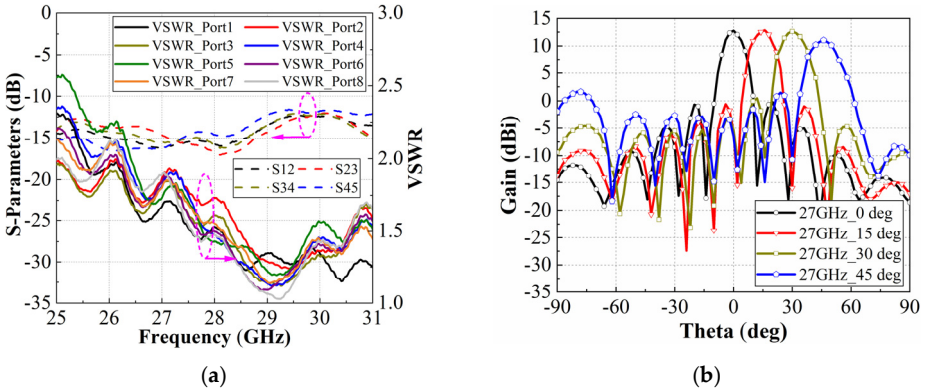

Figure 13. *Cont.*

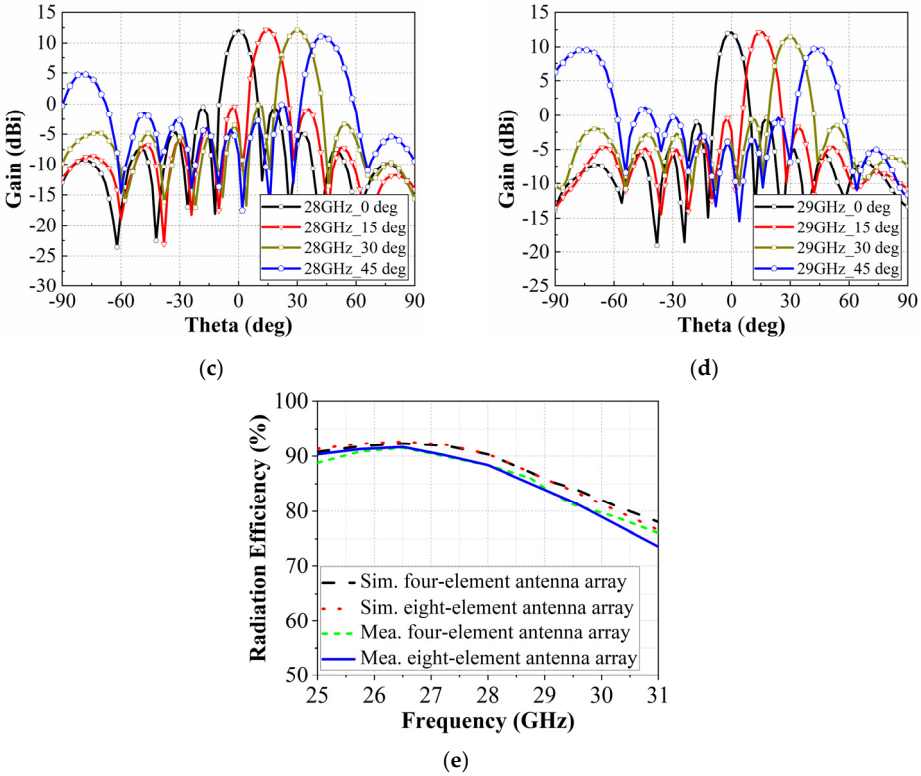

Figure 13. Measured results of the eight-element antenna array. (**a**) S-parameters. Beam-steering at (**b**) 27 GHz, (**c**) 28 GHz, and (**d**) 29 GHz. (**e**) Simulated and measured radiation efficiency.

Table 2. Comparison with other works.

Ref	Bandwidth ($\|S_{11}\| < -10$ dB)	Layer Count	Profile (λ_0)	Element Isolation (dB)	Scanning Angle
[3]	5.3%	2	0.1	20 (typical value)	−54°~44°
[9]	14.8%	2	0.1	≥13 (worst value)	−40°~35°
[11]	10%	8	0.11	/	±45°
[12]	2.46%	4	0.1	/	±45°
This work	17.5%	1	0.07	≥12 (worst value)	±45°

Beyond standalone operation, the designed antenna array also exhibits strong scalability for integration with beamforming chipsets or modules. Figure 14 illustrates a conceptual integration with an RFIC beamforming module. The input signal is processed at the baseband level, followed by digital-domain beamforming, analog-to-digital conversion (ADC), and transceiver (Tx/Rx) operations, before being radiated through the array for beam-steering. The compact 1 × 4 array configuration supports high-density RFIC integration, simplifies feed network design, and enables precise phase control. By contrast, the 1 × 8 array provides higher gain and narrower beamwidth but imposes stricter requirements on interconnect length and layout accuracy, thereby increasing integration complexity. Additionally, maintaining inter-element coupling below −12 dB minimizes mutual interference, ensuring stable beamforming and mitigating distortion effects in multi-channel RFICs. This feature is particularly critical for advanced mmWave phased arrays, enabling reliable high-quality beam-scanning and directional control.

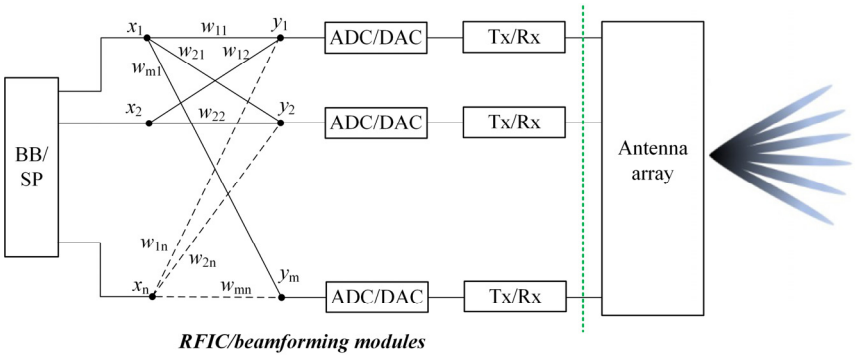

Figure 14. The integration of RFIC/beamforming module and antenna array.

4. Conclusions

In this work, a low-profile mmWave antenna unit with a simple structure was investigated for 5G applications. The design was further extended to four- and eight-element array configurations, whose beam-scanning performances were experimentally characterized using a versatile beam box instrument to provide the required phase excitations. The measured results exhibit satisfactory beam-steering capability across the 5G mmWave n257 band (26.5–29.5 GHz), showing good agreement with simulations. These findings confirm that the proposed design offers a promising and cost-effective solution for future mmWave communication systems.

Author Contributions: Conceptualization, G.-L.H. and C.-Y.-D.S.; methodology, Z.-Y.P. and Y.-J.C.; software, M.-F.X., J.W. and Y.-J.C.; validation, Z.-Y.P., M.-F.X. and J.W.; formal analysis, G.-L.H. and Z.-Y.P.; investigation, G.-L.H., M.-F.X. and J.W.; resources, S.-W.C.; writing—original draft preparation, M.-F.X., J.W. and Z.-Y.P.; writing—review and editing, M.-F.X., G.-L.H., C.-Y.-D.S., W.L. and Y.V.; supervision, C.-Y.-D.S., W.L. and Y.V.; project administration, G.-L.H. and C.-Y.-D.S.; funding acquisition, C.-Y.-D.S. and G.-L.H. All authors have read and agreed to the published version of the manuscript.

Funding: This work was supported in part by NSTC of Taiwan under Grant No. 114-2221-E-110-081, and it is also partially supported by the Sixth Generation Communication and Sensing Research Center funded by the Higher Education SPROUT Project, the Ministry of Education of Taiwan. It is also supported in part by the Guangdong S&T Program Under Grant No. 2024TQ08X647 and Grant No. 2023A1515030114.

Data Availability Statement: The data that support the findings of this study are available from the corresponding author upon reasonable request.

Conflicts of Interest: S.-W.C. was employed by the company TMY Technology Inc. The remaining authors declare that the research was conducted in the absence of any commercial or financial relationships that could be construed as a potential conflict of interest.

References

1. Zhao, L.L.; Zhu, H.L.; Di, Y.J.; Zhao, H.L.; Mou, J.C.; Hu, C.F. Design of joinable antenna array with wide-angle scanning. *IEEE Antennas Wirel. Propag. Lett.* **2025**, *24*, 479–483. [CrossRef]
2. Chen, R.-S.; Huang, G.-L.; Wong, S.-W.; Al-Nuaimi, M.K.T.; Tam, K.-W.; Choi, W.-W. Bandwidth-enhanced circularly-polarized slot antenna and array under two pairs of degenerate modes in a single resonant cavity. *IEEE Antennas Wirel. Propag. Lett.* **2023**, *22*, 288–292. [CrossRef]
3. Zhang, J.; Zhao, K.; Wang, L.; Zhang, S.; Pedersen, G.F. Dual-polarized phased array with endfire radiation for 5G handset applications. *IEEE Trans. Antennas Propag.* **2020**, *68*, 3277–3282. [CrossRef]
4. Chen, R.-S.; Li, X.-D.; Liu, H.-L.; Huang, G.-L.; Wong, S.-W.; Al-Nuaimi, M.K.T.; Tam, K.-W.; Choi, W.-W. Reconfigurable full-metal circularly-polarized cavity-backed slot antenna and array with frequency and polarization agility. *IEEE Trans. Circuits Syst. II Express Br.* **2023**, *70*, 531–535. [CrossRef]

5. Wang, W.; Wu, Y.; Wang, W.; Yang, Y. Isolation enhancement in dual-band monopole antenna for 5G applications. *IEEE Trans. Circuits Syst. II Express Br.* **2020**, *68*, 1867–1871. [CrossRef]
6. Xun, M.; Yang, W.; Feng, W.; Zhang, Y.; Xue, Q.; Che, W.Q. A differentially fed dual-polarized filtering patch antenna with good stopband suppression. *IEEE Trans. Circuits Syst. II Express Br.* **2021**, *68*, 1228–1232. [CrossRef]
7. Tian, H.L.; Chen, Z.J.; Chang, L.; Wang, R.L.; Wang, S.F.; Liu, H.W.; Du, C.; Zhou, D.; Ma, Z.W. Differentially fed duplex filtering dielectric resonator antenna with high isolation and CM suppression. *IEEE Trans. Circuits Syst. II Express Br.* **2022**, *69*, 979–983. [CrossRef]
8. Zhang, S.; Syrytsin, I.; Pedersen, G.F. Compact beam-steerable antenna array with two passive parasitic elements for 5G mobile terminals at 28 GHz. *IEEE Trans. Antennas Propag.* **2018**, *66*, 5193–5203. [CrossRef]
9. Zhao, L.L.; Zhu, H.L.; Ding, C.; Liu, G.Y.; Zhao, H.L.; Mou, J.C.; Guo, Y.J. An ultrawideband dual-polarized tightly coupled dipole array (TCDA) with wide scanning range. *IEEE Antennas Wirel. Propag. Lett.* **2024**, *23*, 1961–1965. [CrossRef]
10. Yang, S.J.; Pan, Y.M.; Shi, L.-Y.; Zhang, X.Y. Millimeter-wave dual-polarized filtering antenna for 5G application. *IEEE Trans. Antennas Propag.* **2020**, *68*, 5114–5121. [CrossRef]
11. Park, J.; Seong, H.; Whang, Y.N.; Hong, W. Energy-efficient 5G phased arrays incorporating vertically polarized endfire planar folded slot antenna for mmWave mobile terminals. *IEEE Trans. Antennas Propag.* **2020**, *68*, 230–241. [CrossRef]
12. Park, J.; Choi, D.; Hong, W. Millimeter-wave phased-array antenna-in-package (AiP) using stamped metal process for enhanced heat dissipation. *IEEE Antennas Wirel. Propag. Lett.* **2019**, *18*, 2355–2359. [CrossRef]
13. TMYTEK. BBox 5G Beamformer Development Platform. TMYTEK Official Website. 2025. Available online: https://www.tmytek.com/products/beamformers/bbox (accessed on 24 August 2025).